Published in final edited form as:
*Eur J Neurosci*. 2019 June 01; 49(11): 1436–1453. doi:10.1111/ejn.14332.

# A Sam68-dependent alternative splicing program shapes postsynaptic protein complexes

**Harald Witte**[1], **Dietmar Schreiner**[1,2], **Peter Scheiffele**[1]

[1]Biozentrum of the University of Basel, 4056 Basel, Switzerland [2]Institute of Neuroanatomy and Cell Biology, 30625 Hannover, Germany

## Abstract

Alternative splicing is one of the key mechanisms to increase the diversity of cellular transcriptomes, thereby expanding the coding capacity of the genome. This diversity is of particular importance in the nervous system with its elaborated cellular networks. Sam68, a member of the Signal Transduction Associated RNA-binding (STAR) family of RNA-binding proteins, is expressed in the developing and mature nervous system but its neuronal functions are poorly understood. Here, we perform genome-wide mapping of the Sam68-dependent alternative splicing program in mice. We find that Sam68 is required for the regulation of a set of alternative splicing events in pre-mRNAs encoding several postsynaptic scaffolding molecules that are central to the function of GABAergic and glutamatergic synapses. These components include Collybistin (*Arhgef9*), Gephyrin (*Gphn*), and Densin-180 (*Lrrc7*). Sam68-regulated Lrrc7 variants engage in differential protein interactions with signalling proteins, thus, highlighting a contribution of the Sam68 splicing program to shaping synaptic complexes. These findings suggest an important role for Sam68-dependent alternative splicing in the regulation of synapses in the central nervous system.

### Keywords

RNA binding protein; synaptic scaffold; mouse hippocampus; dendritic spine; synapse specification



Correspondence: Peter Scheiffele, Biozentrum of the University of Basel, Klingelbergstrasse 50-70, 4056 Basel, Switzerland, peter.scheiffele@unibas.ch.

**Competing interests**
The authors declare no conflict of interest.

***Author contributions***
H.W., D.S. and P.S. designed the study. H.W. and D.S. conducted the experiments and performed data analysis. H.W. and D.S. designed the figures. H.W. and P.S. wrote the manuscript. H.W., D.S., and P.S. revised the manuscript.

**Data sharing**
Raw sequencing data is available at the European Nucleotide Archive ENA under accession number PRJEB27529 (https://www.ebi.ac.uk/ena). All detailed descriptions of DNA constructs and all renewable reagents are available upon request to the authors.


Europe PMC Funders Author Manuscripts

## Introduction

One of the hallmarks of nervous systems is the complexity and precision of neuronal connectivity. During development, large numbers of distinct neuronal cell types are joined into networks with tightly tuned connectivity and function. Recent studies demonstrated that many fundamental aspects of cellular morphologies and initial network connectivity occur independently of neurotransmitter release, thus, indicating that these developmental steps largely proceed through molecularly hardwired mechanisms (Sando et al., 2017; Sigler et al., 2017). Given the vast number and diversity of cells in the central nervous system, the establishment and maintenance of functional networks requires a large number of scaffold and cell adhesion molecules. In this respect, one means to increase the limited coding power of genomes is alternative splicing (Mauger and Scheiffele, 2017; Nilsen and Graveley, 2010; Wang et al., 2008; Zheng and Black, 2013). From some genes, like the *Drosophila* Downs Syndrome Cell Adhesion Molecule (*Dscam1*) and the mouse neurexins (*Nrxn*), thousands of cell surface recognition molecules are generated through alternative splicing (Schmucker et al., 2000; Schreiner et al., 2014; Sun et al., 2013). Importantly, these splice variants are functionally important as they encode self-recognition and synapse specification, respectively (Aoto et al., 2013; Hattori et al., 2007; Matthews et al., 2007; Nguyen et al., 2016; Traunmüller et al., 2016). Moreover, disruptions in alternative splicing programs have been linked to disease states resulting from neuronal network dysfunction, such as autism spectrum disorders (Parikshak et al., 2016; Quesnel-Vallieres et al., 2016). Thus, neuronal splicing programs may more broadly encode cell- and synapse-specific properties (Furlanis and Scheiffele, 2018).

Several RNA binding proteins have been reported to play an important role in driving specific alternative splicing decisions in the nervous system. These include Nova1/2, nElavl, Mbnl1/2, nSR100/SRRM4, Rbfox1/2, nPTBs, and members of the Signal Transduction Associated RNA binding (STAR) proteins: Sam68, Slm1, and Slm2 (Ehrmann et al., 2013; Iijima et al., 2014; Iijima et al., 2011; Ince-Dunn et al., 2012; Lee et al., 2009; Li et al., 2014; Makeyev et al., 2007; Quesnel-Vallieres et al., 2015; Raj and Blencowe, 2015; Saito et al., 2016; Traunmüller et al., 2016; Ule et al., 2003; Ule et al., 2005; Vuong et al., 2016; Wang et al., 2012). Slm1 and Slm2 show cell type-specific expression (Iijima et al., 2014; Nguyen et al., 2016; Stoss et al., 2004; Traunmüller et al., 2014), whereas Sam68 is ubiquitously expressed and functions not only in alternative splicing regulation but also other signalling processes (Chawla et al., 2009; Klein et al., 2013; Sanchez-Jimenez and Sanchez-Margalet, 2013).

In line with its broad expression pattern, previous studies have linked Sam68 dysfunction to multiple pathologies in various tissues, including osteoporosis, infertility, cancer, obesity and ataxia (Vogel and Richard, 2012). In the nervous system, Sam68 has been shown to regulate alternative splicing events in neuronal precursor cells (Chawla et al., 2009) as well as neuronal activity-dependent alternative splicing in mature neurons (Iijima et al., 2011). In addition, cytoplasmic Sam68 has been implicated in the regulation of dendritic mRNAs and the regulation of synaptic plasticity (Grange et al., 2004; Klein et al., 2013). However, despite these important advances, insights into the neuronal functions of Sam68, in particular regarding its mRNA targets, remain limited.

In this work, we performed genome-wide mapping of alternative splicing events in the hippocampus of Sam68 knock-out (*Sam68*$^{KO}$) mice. We uncover the de-regulation of alternative splicing in several key components of both GABA/glycinergic and glutamatergic postsynaptic scaffolds, including Collybistin (*Arhgef9*), Gephyrin (*Gphn*), and Densin-180 (*Lrrc7*). The Sam68-dependent alternative splice variants of Densin 180 exhibit differential interaction with activated Calmodulin-dependent kinase 2 and additional binding partners. Thus, the Sam68-dependent splice isoforms may differentially control synaptic signalling and plasticity. We further compared alternative splicing events dependent on Sam68 with events dependent on Slm2, a closely-related STAR family member with similar RNA binding properties. Despite the pronounced homology between Sam68 and Slm2, the splicing events dependent on either of the two proteins show very little overlap. Thus, there is substantial protein- and context-dependent regulation of alternative splicing that cannot be easily inferred from the presence or absence of RNA-binding motifs. We propose that alternative splicing functions of nuclear Sam68 contribute to the regulation of synapse composition in the central nervous system.

## Materials and methods

### Mice

All procedures involving animals were approved by and performed in accordance with the guidelines of the Kantonales Veterinäramt Basel-Stadt. Accordingly, measures were taken to minimize pain and discomfort of the animals. *Sam68*$^{KO}$ mice were previously described (Richard *et al.*, 2005) and kept in a C57BL/6JRj background (backcrossed for >10 generations). To reduce the increased perinatal lethality described for *Sam68*$^{KO}$ mice (Richard et al., 2005), littermate (WT and *Sam68*$^{KO}$) male offspring (F2) of RjOrl:SWISS X B6 hybrid heterozygous (*Sam68*$^{+/-}$) females (F1) and heterozygous (*Sam68*$^{+/-}$) C57BL/6JRj males was used for the analysis of spine morphology.

Sample sizes were determined based on previous experience with the manipulations, advice from colleagues, and literature surveys. A formal sample size calculation was not performed as the effect sizes were unknown during the time of study design. Animals that differed by 20% in weight from the mean of the group or that exhibit visible behavioural abnormalities were excluded from the analysis (preestablished criterion). Investigators performing anatomical analysis were blinded to the genotype of the sample.

### RNA isolation and RT-PCR

For RNA isolation, brain tissue was dissected in ice-cold 1xPBS, homogenized in 1 ml TRI Reagent (Sigma #T9424) and thoroughly mixed with 200 µl chloroform (Sigma #2432). After three minutes incubation at room temperature samples were centrifuged at 16’000 g, +4°C for 15 min. The aqueous phase was used for RNA purification with the RNeasy Plus Mini kit (Qiagen #74134) following the manufacturer’s instructions, including on-column DNase-treatment to remove traces of genomic DNA. 1 µg of total RNA was reverse transcribed using random hexamers (Promega #C1181) and ImProm II reverse transcriptase (Promega #A3802).

### Illumina paired-end sequencing and data analysis

RNA-Seq and alternative splicing analysis anlysis was done as previously described (Traunmüller et al., 2016). Total hippocampal RNA was extracted with TRI Reagent (Sigma #T9424) and purified using Qiagen RNeasy Plus Mini Kit including on-column DNase-treatment as described above. Total RNA was quality-checked on a Bioanalyzer instrument using RNA 6000 Nano Chips and quantified by spectrophotometry. Library preparation was performed with 1µg total RNA using the TruSeq PolyA+ Stranded mRNA Library Prep Kit. Libraries were quality-checked on a Fragment Analyzer using the Standard Sensitivity NGS Fragment Analysis Kit revealing excellent quality of libraries. The eight samples (4x WT, 4x *Sam68*$^{KO}$) were pooled to equal molarity. Each pool was run on a Fragment Analyzer for quality-check and quantification purposes in order to be adjusted to 12pM and used for clustering on the cBot2. Samples were sequenced Paired-end over 100 cycles on HiSeq2500. Primary data analysis was performed with the Illumina RTA version 1.18.64 and bcl2fastq-2.16.0.10. Primary RNA-Seq data analysis was performed by Dr. Pierre de la Grange (GenoSplice, France). Sequencing, data quality, reads repartition, and insert size estimation were performed using FastQC, Picard-Tools, Samtools and rseqc. Reads were mapped using STARv2.4.0 (Dobin et al., 2013). Gene expression was estimated as described (Noli et al., 2015) using Mouse FAST DB v2015_1 annotations. Only genes expressed in at least *Sam68*$^{KO}$ or WT were further analyzed. Genes were considered as expressed if their rpkm value was greater than the background rpkm value based on intergenic regions. Analysis at the splicing level was first performed taking into account only exon reads and flanking exon-exon junction reads (“EXON” analysis) in order to potentially detect new alternative events that could be differentially regulated (i.e., without taking into account known alternative events). In particular, all microexons from FAST DB annotations are analyzed, even if they have not been already described as alternative exons. The Mouse FAST DB 2015_1 annotations contain 4,926 microexons (from 3 to 27bp), including 1,515 internal microexons (i.e., not first or terminal gene exons). Three of the 4,926 microexons were significantly altered in the *Sam68*$^{KO}$ datasets as compared to WT (Hira exon3, Ptprz exon 16 and Sgce exon 9). Analysis at the splicing level was also performed by taking into account known patterns (“PATTERN” analysis) using the FAST DB splicing patterns annotation (i.e., for each gene, all possible splicing patterns were defined by comparing exon content of transcripts). All types of alternative events can be analyzed: Alternative first exons, alternative terminal exons, cassette exon, mutually exclusive exons, alternative 5’ donor splice site, alternative 3’ acceptor splice sites, intron retention, internal exon deletion and complex events corresponding to mix of several alternative event categories). “EXON” and “PATTERN” analyses were based on the splicing-index calculation as previously described (Gandoura et al., 2013). Results were considered statistically significant for P-values ≤ 0.05 and fold-changes ≥ 1.50. Finally, significant results from “EXON” and “PATTERN” analyses were merged to obtain a single result list.

Predictions by this computational pipeline were validated previously by PCR-based methods (Traunmüller et al., 2016). For the present dataset, a validation rate of >90% was confirmed by PCR assays for 13 selected targets: *Arhgef9, Cap1, Epha6, Dlgap, Gephn, Gria2, Hdac1, Homer1a, Lrrc7, Lrrtm1, Nrxn1, Usp15*. One predicted intron retention event in *Ube3a* could not be validated in the assays performed. We note that the alterations in *Hdac1* need to

be interpreted with caution as this gene lies in direct proximity to the Sam68 locus and may be affected by strain-specific alterations (arising from the 129/SvJ strain background used for original generation of the mice which may not be removed even with extensive backcrossing).

For statistical analysis of differential gene expression, parametric Wald test is applied by DESeq, with multiple testing correction using the Benjamini-Hochberg method for p-value adjustment (Benjamini and Hochberg, 1995). T-test is used for statistical analysis of alternative splicing as previously described (Traunmüller et al., 2016).

Raw sequencing data was deposited at the European Nucleotide Archive ENA under accession number PRJEB27529 (https://www.ebi.ac.uk/ena).

## Alternative splicing analysis by RT-PCR

For experimental validation of analyzed RNA-Seq data, DNA amounts and PCR cycle numbers were carefully titrated to ensure correct amplification range in RT-PCRs. Sequences of PCR primers were as follows:

| Name | Sequence (5’-3’) |
|---|---|
| Arhgef9_ex8_fwd | GACAGGCTGCAATGACTGTG |
| Arhgef9_ex10_rev | TGGTTTAACGGGTCCTGTGG |
| Gapdh_fwd | GCTTGTCATCAACGGGAAG |
| Gapdh_rev | TTGTCATATTTCTCGTGGTTCA |
| Gphn_ex8_fwd | GAGACACAGCCTCCCTTAGC |
| Gphn_ex11_rev | TGCTGCACCTGGACTGG |
| Lrrc7_ex22_fwd | CAAACCAGGCCAGTTTCAGC |
| Lrrc7_ex27_rev | TATCCCCGGGCTGTAGTAGG |
| Nrxn1_AS4_fwd | TGTTGGGACAGATGACATCGCC |
| Nrxn1_AS4_rev | GAGAGCTGGCCCTGGAAGGG |

## Lrrc7-pulldown assay

Full-length Lrrc7 splice variants missing or containing alternative exons 23 and 24 (stable exon ID: ENSMUSE00000668385 and ENSMUSE00000440890, respectively) were cloned from hippocampal cDNA into pEGFP-C1 and expressed in HEK293T cells (ATCC #CRL-3216) for two days. Empty pEGFP-C1 was used as a negative control. HEK293T cells expressing GFP-tagged Lrrc7 isoforms were collected in ice-cold 1x PBS and lysed for 10min at +4°C in lysis buffer (150mM NaCl, 50mM Tris-HCl pH 7.5, 5% glycerol, 1% TX-100, 5mM NaF) supplemented with 1x cOmplete EDTA-free Protease inhibitor cocktail (Roche #11836170001) and 1x PhosSTOP phosphatase inhibitor cocktail (Roche #04906837001) using sonication (Hielscher Vial Tweeter). The resulting lysate was incubated for 10 min at +4°C on a rotator, spun for 10 min at 20’000 g at +4°C and the resulting supernatant was used further. Biotinylated single-chain anti GFP nanobody was coupled to magnetic streptavidin beads (Pierce #88816), excess nanobody was removed by washing 2x with ice-cold lysis buffer, then incubated on a rotator for 1-2 h at +4°C with the

GFP-Lrrc7-containing HEK293T cell lysate to isolate GFP-Lrrc7 isoforms on the magnetic beads (Lrrc7-beads) and subsequently washed 3x with ice-cold lysis buffer. In parallel, total brain lysate of adult male C57BL/6JRj mice (12-16 weeks old) was prepared using 15 ml lysis buffer per gram tissue in a Dounce glass homogenizer, incubated on a rotator for 10 min at +4°C, and spun for 10 min at 20'000 g at +4°C. The soluble supernatant was filtered through a 0.45 μm-filter to further clarify the brain lysate and then incubated with Lrrc7-beads overnight at +4°C on a rotator. The next morning Lrrc7-beads were washed 3x with 1x ice-cold lysis buffer and 1x with ice-cold 1x PBS. Beads were split and bound proteins either eluted using 1% sodium deoxycholate (Sigma #30970) in 50mM ammonium bicarbonate (Sigma #A6141) for mass spectrometry analysis or directly in 1x protein loading buffer (50mM Tris-HCl pH 6.8, 2% SDS, 100mM DTT, 10% glycerol, 0.012% bromphenol blue) for Western Blot. Elution was aided by incubating the beads for 5 min at 50°C or 95°C for mass spectrometry or Western Blot analysis, respectively.

## Antibodies, dyes and and Western Blot

Polyclonal antibodies for SAM68, SLM1, and SLM2 have been previously described and validated (Iijima et al., 2011). In brief, polyclonal antibodies were raised in rabbits and guinea pigs using the following synthetic peptides: RGVPPPPTVRGAPTPRAR-(C) (anti-SAM68), VNEDAYDSYAPEEWAT -(KKKC) (anti-SLM1), and PRARGVPPTGYRP-(C) (anti-SLM2). The residues in brackets were added for coupling and to improve the solubility of the peptide. Antibodies were affinity-purified from serum on the antigens. Polyclonal anti-GFP antibodies generated in rabbits and affinity purified using recombinant EGFP produced in *E. coli* have been descried before (Taniguchi et al., 2007). The following commercially available antibodies and dyes were used in this study: mouse anti beta3-tubulin (Tuj-1; Covance #Co-MMS-435P-250), rabbit anti Calnexin (StressGen #SPA-865); rabbit anti Gapdh (Cell Signaling #5174); mouse anti CaMKII alpha (Thermo Fisher Scientific #MA1-048); mouse anti phospho Thr 286-CaMKII alpha (Thermo Fisher Scientific #MA1-047); rabbit anti Cyfip1 (Millipore #07-531); rabbit anti Cadherin 10 (Abcam #ab134137).

Fluorophore-coupled secondary antibodies were from Life Technologies (Alexa Fluor 488 donkey anti-mouse #A-21202; Alexa Fluor 568 donkey anti-rabbit #A10042). Hoechst 33342 dye (Sigma #B2261) was used for nuclear staining.

Secondary antibodies coupled to horse radish peroxidase (HRP) were from Jackson ImmunoResearch (goat anti-rabbit HRP #111-035-003; goat anti-mouse #115-035-174). For enhanced chemiluminescence detection, WesternBright ECL kit (Advansta #K-12045-D20) was used.

## Dissociated hippocampal neurons

Hippocampi from E18.5 or P0 animals were dissected, trypsinized for 12min in 0.05% trypsin (Gibco #25300) buffered with 10mM HEPES (Gibco #15630) at 37°C, washed 3x with HBSS (Gibco #14025) buffered with 10mM HEPES (Gibco #15630) and titurated using a fire-polished glass Pasteur pipette. Cells were plated at a density of 10-12'000 cells per $cm^2$ on poly-D-lysine (Sigma #P7886)-coated glass coverslips (Marienfeld #0111520 or

0111550) in DMEM (Sigma #D5796) containing 1% Penicillin/Streptomycin (Sigma #P4333) and 10% fetal bovine serum (Gibco #10270). 4-6 h after plating, media was changed to serum-free Neurobasal media (Gibco #21103) supplemented with 2 mM GlutaMax (Gibco #35050) and B27 supplement (Gibco #17504). Cells were then grown at 37°C / 5% $CO_2$.

### Immunocytochemistry

Cells were fixed for 15 min using 4% PFA / sucrose in 100mM phosphate buffer pH 7.5 at room temperature (RT), washed 3x with 1x PBS, permeabilized for 5 min with 1x PBS containing 0.1% TX-100 and blocked for 1h at RT with blocking solution (mix of 2% FBS (Gibco #10270) / 2% bovine serum albumin (Sigma #A9647) / 2% donkey serum (Jackson ImmunoResearch #017-000-121) / 0.4% fish gelatine (Sigma #G7765) in 1x PBS).

In subsequent steps, antibodies were diluted in 10% blocking solution in 1x PBS and 0.1% TX-100. Primary antibodies were applied for 1-2 h at RT or overnight at +4°C. After 4 washes with 1x PBS, fluorophore-coupled secondary antibodies were applied 30-45 min at RT. Cells were then washed 3x with 1x PBS, once with deionized water, mounted using Fluoromunt G (Southern Biotech #0100-01), and dried at RT. Hoechst dye was co-applied with secondary antibodies at a final concentration of 0.5 µg/ml. Stained cells were imaged on a Zeiss LSM 700 confocal microscope using 10x or 63x Plan-Apochromat objectives (numerical aperture 0.45 and 1.40, respectively).

### DiOlistic labelling

Diolistic labeling with DiI (Molecular Probes #D282) was performed as previously described (Gan et al., 2000; Staffend and Meisel, 2011). Images were acquired on an upright LSM700 confocal microscope (Zeiss) controlled by Zen 2010 software, using 10x or 63x Plan-Apochromat objectives (numerical aperture 0.45 or 1.40, respectively). For spine counting, confocal image stacks (0.13µm optical sections, 63x objective, 2x zoom) of higher-order dendritic branches in the stratum radiatum of CA1 pyramidal neurons were acquired. Spines were counted per length of dendritic segment evaluated by assessing the 3D information of the confocal image stacks using ImageJ. Headed and non-headed spines were distinguished manually. All assessments were performed by an investigator blinded to the genotype of the respective samples.

### Overrepresentation assay

Analysis of GO terms was done using the statistical overrepresentation test (Mi et al., 2013) of the PANTHER classification system (release 20171205), available on http://pantherdb.org/. Genes showing significant alternative splicing events (FC ≥ 1.50; $p \leq 0.05$) were analysed using the GO cellular component annotation data set and Fisher's Exact test with false discovery rate correction for multiple testing. As reference list, all genes expressed in the deep sequencing data set were used.

### Binding motif enrichment

Frequency of Sam68 binding motifs (AUAAAA;(Ray et al., 2013) was assessed using the RBPmap web server [http://rbpmap.technion.ac.il/;(Paz et al., 2014)], using high stringency

level and applying the conservation filter. The number of non-overlapping motifs was counted 500bp up- and downstream of alternatively spliced segments regulated by Sam68 as well as of a set of 359 control exons comparable in size to the Sam68-regulated exons. Control exons were selected from all exons expressed in the RNA sequencing data set (alternative-splicing regulation by Sam68 <2% FC SI, size range within ±5% of Sam68-regulated exons). For motif enrichment, the ratio of the average motif count for Sam68-regulated and control exons was calculated. For statistical analysis, a permutation test was used (50'000 Monte Carlo replications) to reveal the distribution of motif enrichment scores. The quantiles of this distribution were used to determine the significance level of the observed enrichment.

### Mass spectrometry analysis and label-free quantification

For carbamidomethylation of cysteines, samples were shaken at 37°C for 1h in Tris-(2-carboxyethyl)- phosphine hydrochloride (TCEP, 1:40 v:v), alkylated in iodoacetamide at RT for 30min in the dark (1:40 v:v) and then incubated with N-acetyl-cysteine at RT for 10min. Subsequently, samples were digested overnight at 37° with trypsin (1µg). The resulting peptides were purified and desalted using MicroSpin C18 silica columns (The Nest Group, MA, USA #SEM SS18V) according to the manufacturer's instructions, dried under vacuum, resuspended in LC Buffer A (2% acetonitrile 0.15% formic acid) and stored at -80°C until further processing.

From each sample, 1µg of peptide was subjected to LC–MS analysis using a dual pressure LTQ-Orbitrap Elite mass spectrometer (Thermo Fisher Scientific) connected to an electrospray ion source (Thermo Fisher Scientific) as described (Glatter et al., 2012). Peptide separation was carried out on an EASY nLC-1000 system (Thermo Fisher Scientific) equipped with a RP-HPLC column (75 µm × 30 cm) packed in-house with C18 resin (ReproSil-Pur C18–AQ, 1.9 µm resin, Dr. Maisch GmbH). A linear gradient from 95% solvent A (0.15% formic acid, 2% acetonitrile) and 5% solvent B (98% acetonitrile, 0.15% formic acid) to 28% solvent B over 90 min at a flow rate of 0.2 µl/min was used. Data acquisition mode was set to obtain one high resolution MS scan in the FT part of the mass spectrometer at a resolution of 120,000 full widths at half-maximum (at m/z 400) followed by 10 MS/MS scans in the linear ion trap of the most intense ions (TOP10) using rapid scan speed. Unassigned and singly charged ions were excluded from analysis and dynamic exclusion duration was set to 30 s.

MS1-based label-free quantification of MS data was performed using Progenesis QI software (Nonlinear Dynamics (Waters), version 2.0). MS raw files were imported into Progenesis QI software and analyzed using the default parameter settings. MS/MS-data were exported from the software in "mgf" format and searched with a target/decoy strategy by MASCOT (version 2.4.1) against a database containing forward and reverse sequences of the proteome from *Mus musculus* (UniProt, 33,984 entries) using. Search criteria required full tryptic specificity allowing for three missed cleavages. Carbamidomethylation of cysteine was specified in Mascot as a fixed modification. Oxidation of methionine and acetylation of the N-terminus were specified in Mascot as variable modifications. Mass tolerance was set to 10 ppm for precursor ions and 0.6 Da for fragment ions. The peptide

and protein false discovery rate (FDR) was set to 1%. Results from the database search were imported into Progenesis QI and the resulting peptide measurement list containing peak area values of identified peptides was exported. Processing and statistical evaluation of peptide and protein quantities between samples was performed using SafeQuant (Glatter et al., 2012). Normalized peptide and protein intensities from SafeQuant analysis were used to calculate intensity ratios, log2 ratios and q values between experimental conditions for identified proteins.

SAINT analysis (significance analysis of interactome) was carried out using SAINTexpress (v. 3.6) (Choi et al., 2011), using spectral counts as input data. The results were filtered to only include interaction partners assigned a Bayesian False Discovery Rate (BFDR) < 0.01.

The subset of Lrrc7 interactors derived from SAINT analysis was re-evaluated by label-free quantification as described above to identify a list of Lrrc7 isoform-specific interaction partners. To this end, results from the *Mus musculus*-proteome database search were imported into Progenesis. The database search results were filtered, (1) limiting the peptide and protein level FDR to 1% and (2) to only include the list of LRRC7 interaction partners identified using SAINTexpress (v. 3.6). The Progenesis analysis results were further processed using the SafeQuant R package (Ahrne et al., 2016), to obtain protein relative abundances. This analysis included data normalization (based on the peak areas of LRRC7 peptides common to all isoforms), summation of MS1 peak areas per protein and LC-MS/MS run, followed by calculation of protein abundance ratios and testing for differential abundance using empirical Bayes method. The resulting p-values, reflecting the probability of detecting a given mean abundance difference across sample conditions by chance alone, were corrected for multiple testing using the Benjamini-Hochberg method (Benjamini and Hochberg, 1995). The final list of LRRC7 isoform specific interaction partners include those proteins that were found to be significantly differentially abundant (adjusted p-value < 0.05, fold-change ≥ 20%) in at least one bait-bait condition comparison.

## Results

### Genome-wide mapping of Sam68-dependent alternative splicing

Previous work reported nuclear and cytoplasmic functions for Sam68 (Chawla et al., 2009; Grange et al., 2004; Iijima et al., 2011; Klein et al., 2013; Matter et al., 2002; Paronetto et al., 2007). To begin to investigate the functions of Sam68 in the mouse hippocampus, we assessed its localization in cultured hippocampal neurons. In line with previous studies we detected the vast majority of Sam68-immunoreactivity in the nucleus (Fig. 1A, B). The specificity of our immunological reagents was confirmed with immunostainings on hippocampal cultures prepared from Sam68 knock-out (*Sam68*$^{KO}$) mice (Fig. 1B) and probing of lysates from adult mouse hippocampus (Fig. 1C). The nuclear immunoreactivity was almost completely abolished in Sam68 knock-out cultures (Fig. 1B). Only very low signals remained in the cells, and we conclude that these remnants of immunoreactivity represent background due to unspecific interactions.

For a genome-wide identification of transcripts that depend on Sam68 expression in the hippocampus we performed RNA sequencing of poly-adenylated RNAs isolated from wild-

type (WT) and knock-out (KO) hippocampi (n=4 for both WT and *Sam68*$^{KO}$, postnatal day 30 (P30) males). We obtained 150-200 Mio paired-end reads for each replicate. Of these, 84-87% uniquely mapped to the mouse genome and only <0.5% mapped to ribosomal RNAs. Quantitative comparison of gene expression between *Sam68*$^{KO}$ and WT hippocampus uncovered only very modest changes in overall transcript levels. Transcripts from ten loci were more than 2-fold upregulated (including *Oacyl* and *Mir 219-a2*) whereas transcripts from 26 loci were found to be down-regulated more than 2-fold in the mutant mice, amongst them Sam68/*Khdrbs1* itself, *Iqcc*, and *Sdf2l1* (Fig. 2A, adjusted p-value cut-off for all p<0.05; Supplementary Data 1).

We next assessed changes in alternative splicing events on a genome-wide level. Using cut-offs of 1.5 fold-change (FC) in splicing index (SI) and p-value <0.05 we identified 73 altered alternative splicing events in *Sam68*$^{KO}$ compared to WT (Fig. 2B, Supplementary Data 2). In about 60% of the events inclusion of the alternatively spliced segments is increased in *Sam68*$^{KO}$ (Fig. 2C). This is consistent with a role for Sam68 in promoting exon skipping. Cassette exon splicing (e.g. for *Lrrc7, Epha6*, or *Kif21a*), usage of alternative terminal exons (e.g. for *Dlgap1*, *Gria2* or *Lrrtm1*), or intron retention (e.g. for *Arhgef9* or *Cacnb3*) constituted the majority of events with increased inclusion. For events with decreased inclusion, changes in cassette exon splicing (e.g. for *Gphn*, *Sorbs1*, or *Sorbs2*) and alternative terminal exons (e.g. for *Homer1* or *Hdac1*) were observed as well, in addition the usage of alternative 3'- (e.g. for *Dhdds* or *Ank3*) or 5'-splice sites (e.g. for *Celf3* or *Szt2*) was observed (Fig. 2C).

For several RNA binding proteins, alternative splicing programs have been shown to control transcript levels by generating transcript isoforms that are targeted by nonsense-mediated decay (Eom et al., 2013; McGlincy and Smith, 2008; Yap et al., 2012). However, the majority of transcripts with significantly changed alternative splicing events displayed overall minor expression level changes of (less than 20%) between wild-type and *Sam68*$^{KO}$ mice (Fig. 3A). Thus, the impact of Sam68 -dependent alternative splicing on transcript abundance is low. Given the ubiquitous expression of Sam68, we examined whether the putative Sam68 alternative splicing targets are expressed in neurons or rather in other hippocampal cell types. We compared expression levels of Sam68-regulated transcripts in neurons, astrocytes, endothelial cells, microglia, and myelinating oligodendrocytes (using transcript data from (Zhang et al., 2014)). A large fraction of genes with Sam68-dependent splicing events was preferentially expressed in neurons (Fig. 3B). In addition, a subset of Sam68-dependent transcripts exhibited higher expression in other cells types. This supports a role for Sam68 in the regulation of alternative splicing in neurons as well as other cell types in the mouse hippocampus. Gene ontology (GO) analysis provided further support for neuronal functions of Sam68-dependent alternative splicing targets. Statistical analysis (Mi et al., 2013) revealed synapse-related GO-terms to be overrepresented in these Sam68-regulated transcripts (Fig. 3C). This suggests a preferential requirement for Sam68 in the regulation of alternative splicing events in transcripts that encode synaptic proteins, particular components of the postsynaptic density.

### Regulation of postsynaptic scaffolding proteins by Sam68

To further investigate Sam68-dependent alternative splicing regulation of synaptic proteins, we analysed the alternative splicing patterns for several candidate targets encoding key synaptic proteins in the *Sam68*$^{KO}$ hippocampus (Fig. 4A) [Collybistin (*Arhgef9*), Gephyrin (*Gphn*), and Leucine-rich repeat containing protein 7 (*Lrrc7*, also called Densin-180), Neurexin1 (*Nrxn1*)]. We examined several time points across early postnatal development over the time when synaptogenesis proceeds in the mouse hippocampus ((postnatal day 0 to postnatal day 21). During the first three postnatal weeks, *Arhgef9* (exon 11; exon ID ENSMUSE00000817669) and *Lrrc7* (exon 23; ENSMUSE00000668385) showed an increase in exon skipping, whereas *Gphn* (exon 10 which is referred to as the C4a splice cassette [(Fritschy et al., 2008); ENSMUSE00000418916)] and *Nrxn1* (exon 21 at alternatively spliced segment 4 (AS4); ENSMUSE00001309616) showed an increase in exon inclusion (Fig. 4B).

Sam68 as well as other STAR-proteins (Slm1 and Slm2) are highly expressed during these postnatal stages (Fig. 4C). We note that overall Sam68 expression slightly declines over the first 5 postnatal weeks. However, Sam68 activity appears to significantly depend on post-translational modifications (Iijima et al., 2011; Matter et al., 2002; Paronetto et al., 2007). In *Sam68*$^{KO}$ hippocampus, alternative splicing patterns of *Arhgef9* (exon 11), *Gphn* (exon 10/C4a), *Lrrc7* (exon 24; ENSMUSE00000440890), and *Nrxn1* (exon 21 / AS4) were significantly changed, confirming predictions based on the RNAseq analysis [Fig. 4D, arrowheads; Supplementary data 2, RNA-Seq-based changes at P32: *Arhgef9* exon 11, 1.59x up; *Gphn* exon 10/C4a, 1.86x down; *Lrrc7*, exon 24 1.5x up; *Nrxn1* exon 21 (AS4) 1.18x up]. This analysis experimentally confirms the conclusion that Sam68 regulates alternative splicing in transcripts encoding key structural components of both GABAergic and glutamatergic synapses.

### Sam68-dependent splicing events regulate synaptic protein complexes

The alternative segment 4 in *Nrxn1* which we find here to be regulated by Sam68 at P0, depends strongly on the Sam68 paralogue Slm2 at later postnatal stages (Ehrmann et al., 2013; Traunmüller et al., 2014). Alternative splicing at this site directs functional specification of hippocampal synapses and gates trans-synaptic interactions with postsynaptic ligands (Boucard et al., 2005; Chih et al., 2006; Traunmüller et al., 2016). To explore whether additional Sam68-dependent alternative splicing events change synaptic protein complexes we tested the impact on biochemical interactions with binding partners. We focused on Lrrc7 since this protein has emerged as a critical regulator of glutamatergic postsynaptic structure and plasticity (Carlisle et al., 2011; Wang et al., 2017). We performed affinity-isolation of Lrrc7-binding proteins from mouse whole brain lysate using three full-length Lrrc7 isoforms expressed in HEK293 cells as bait. These isoforms differ in the presence (+) or absence (-) of insertions encoded by the Sam68-regulated alternative segment (exon 23/24, resulting in Lrrc7 23-/24-, 23-/24+, and 23+/24+, respectively). Lrrc7 23-/24- is strongly de-regulated in *Sam68*$^{KO}$ hippocampus; 23-/24+ is significantly elevated in *Sam68*$^{KO}$ hippocampus; 23+/24+ is expressed at birth and then down-regulated both in wild-type and knock-out hippocampus (Fig. 4D). As a positive control, we probed immuno-precipitates for calcium/calmodulin-dependent kinase II (CaMKII) alpha, which is known to

interact with these Lrrc7 variants (Strack et al., 2000). We find robust recovery of CaMKII alpha for all three Lrrc7 variants under our experimental conditions (Fig. 5A). Interestingly, the active Thr286-phosphorylated form of CaMKII alpha was preferentially recovered on the 23+/24+ splice variant that is highly expressed in newborn mice and then downregulated over the first 2 postnatal weeks (Fig. 4B; Fig. 5A, B). We next performed an unbiased proteome-wide survey of Lrrc7 binding partners by mass spectrometry. Tryptic peptides from n=4 independent affinity purifications on baits and negative control proteins where analysed by label-free proteomic shotgun analysis. To identify proteins selectively binding to Lrrc7 we used SAINT analysis which models the probability for true protein-bait interactions by comparing the distribution of spectral counts recovered for proteins across replicates from bait versus negative control conditions (Choi et al., 2011). This analysis yielded several common (isoform-independent) Lrrc7-interactors, including previously identified partners CaMKII alpha, beta, gamma and delta, alpha and delta Catenins and Shank1,2,3 proteins (Fig.5C). In addition, we identified several previously unknown Lrrc7-interactors (Fig. 5C; complete list see Supplementary Data 3). These include the phosphodiesterase 4a and the mindbomb E3 ubiquitin ligase 1 which have been implicated in synaptic plasticity (Hansen et al., 2014; Havekes et al., 2016; Yoon et al., 2012). To specifically identify splice isoform-specific interactors, we used the SAINT-filtered list of Lrrc7 binders and assessed their interactions with the different Lrrc7 variants (23-/24-, 23-/24+, 23+/24+, respectively). Notably, several Lrrc7 interaction partners displayed differential retention on the Lrrc7 variants, including the cytoplasmic Fmr1-interacting protein 1 (Cyfip1), the adhesion molecule cadherin 10, and the TNF-receptor associated protein 7 (Traf7) (preferentially binding to the Lrrc7 23+/24+ variant; Fig. 5D-F, Supplementary Data 4). Using Western blots on co-immunoisolates we confirmed isoform-selective Lrrc7-interactions for Cyfip1and Cadherin 10 (Fig. 5E). As judged by the relatively low retention of the proteins on the affinity matrix as compared to the common binding partners CaMK2 and Shank proteins (see Supplementary Data 3 and 4) we conclude that the binding affinities of these ligands are lower than those seen for the previously identified ligands, at least under our experimental conditions. Nevertheless, the proteins did exhibit differential recovery for the LRRC7 variants. Thus, the Sam68-dependent splice isoform choices may indeed regulate specific postsynaptic protein assemblies.

Considering that the set of targets of Sam68-regulated alternative splicing was enriched for genes that control glutamatergic synapse development and properties, we tested whether *Sam68*$^{KO}$ neurons may exhibit alterations in the density or morphology of dendritic spines. We used DiOlistic labelling (Gan et al., 2000; Staffend and Meisel, 2011) on adolescent animals (P32) to visualize individual neurons in sagittal brain sections. We then quantified density and morphology of dendritic spines on higher-order branches of dendrites of CA1 neurons in the *stratum radiatum* (Fig. 6A, B). We observed overall very similar densities of dendritic protrusions in neurons from *Sam68*$^{KO}$ mice and littermate control animals (Fig. 6C). The numbers of both headed and non-headed spine-like protrusions were unchanged (Fig. 6C). Thus, in these preparations, the density and morphological maturation of dendritic spines is not altered by global loss of Sam68.

### Differential dependence of splicing events on Sam68 and its paralogue Slm2

The A-U-rich consensus motif of Sam68 (AUAAAA) has previously been characterized (Lin et al., 1997; Ray et al., 2013). When we assessed the frequency of binding sites in sequences upstream and downstream of the Sam68-dependent exons we found a significant enrichment compared to control exons (1.59x and 2.44x, respectively; p-value <0.05 and <0.001, respectively). Notably, Sam68 and Slm2 are co-expressed in CA1 neurons and interact with the same RNA consensus motif (Lin et al., 1997; Ray et al., 2013). Surprisingly, there was little overlap between splicing events de-regulated in *Sam68*$^{KO}$ and *Slm2*$^{KO}$ hippocampi (Fig. 7A, B). Two commonly de-regulated transcript were *Stxbp5l* and *Nrxn1* AS4, although de-regulation was more severe for *Slm2*$^{KO}$ than for *Sam68*$^{KO}$ (*Stxbp5l* at exon 24; SI FC$^{Sam68}$ = 1.48 and SI FC$^{Slm2}$ = 1.58 and *Nrxn1* AS4 SI FC$^{Sam68}$ = 1.18 and SI FC$^{Slm2}$ = 2.07). When focusing on alternative splicing events severely de-regulated in *Sam68*$^{KO}$ mice (FC SI≥1.5, p<0.05) none of the 73 events showed equivalent changes in *Slm2*$^{KO}$ (Fig 7B, C). Thus, despite recognizing similar RNA motifs, Sam68 and Slm2 proteins do not compensate each other's loss-of-function. This observation indicates that, in addition to the RNA binding motif, also cellular context, presence of cofactors and/or the concentration of the respective RNA-binding protein in a given cell have major impact on the candidate targets recovered in these loss-of-function studies.

## Discussion

In this study, we mapped the SAM68-dependent alternative splicing program and cellular phenotypes in mouse hippocampus. Previous work has shown Sam68 to be involved in various processes including transcription, translation, RNA transport, miRNA processing and alternative splicing (Vogel and Richard, 2012). Sam68 has been reported to regulate alternative splicing events during neurogenesis and to shift alternative splicing of neurexins in response to neuronal activity (Chawla et al., 2009; Iijima et al., 2011). However, a genome-wide mapping of Sam68-dependent splicing events in mature neurons has not been previously performed. We uncover a panel of Sam68-dependent splicing events in mRNAs encoding synaptic proteins which are regulated over postnatal development at a time when synapse formation and maturation proceed.

The synaptic proteins encoded by Sam68-dependent mRNAs include adhesion molecules and synaptic scaffolding proteins of excitatory as well as inhibitory synapses. Gephyrin and Collybistin are two interesting targets as they serve key scaffolding functions at postsynaptic glycinergic and GABAergic sites. The Sam68-dependent gephyrin C4 exon cluster contains multiple alternative exons (C4a through C4d) which may modify oligomerization and/or phosphorylation state (Fritschy et al., 2008; Herweg and Schwarz, 2012). Notably, gephyrin is also alternatively spliced at another cassette (C3) controlled by the splicing factor Nova2 (Ule et al., 2003) which is independent of Sam68. Alternative splicing regulation of collybistin (encoded by *Arhgef9*) produces isoforms that differ in their N- and C-termini (Harvey et al., 2004; Kins et al., 2000). The internal alternatively spliced segment uncovered in our study differs from these previously described sites and may render the transcript isoform subject to nonsense-mediated decay. This adds further complexity to *Arhgef9* transcript regulation. The alternative segment in *Lrrc7* has been implicated in modulating

protein complexes at glutamatergic postsynaptic sites, in particular association with calcium/calmodulin-dependent kinase II (Strack et al., 2000). Moreover, alternative splicing of *Nrxn1* at AS4 controls interactions with multiple synaptic ligands, in particular the glutamatergic proteins neuroligin-1, leucine-rich repeat proteins (LRRTMs), and the Cbln1-GluD2 complex (Chih et al., 2006; de Wit et al., 2009; Ichtchenko et al., 1995; Matsuda et al., 2016; Schreiner et al., 2015; Uemura et al., 2010). Thus, the Sam68-dependent splicing program controls both, glutamatergic and GABAergic synapse components.

In our phenotypic analysis we focused on alterations at glutamatergic synapses, since $Sam68^{KO}$ mice had been reported to exhibit defects in mGluR-dependent long-term depression (Klein et al., 2015). We hypothesize that this phenotype may – at least in part – result from alterations in alternative splicing. Notably, *Lrrc7*, one of the mRNAs the alternative splicing pattern of which we find to be altered in $Sam68^{KO}$ mice, has itself been linked to mGluR signalling. In $Lrrc7^{KO}$ mice, there is a reduction in PSD-association of mGluR5 and a loss of mGluR-dependent long-term depression in the hippocampus (Carlisle et al., 2011). On the other hand, some $Sam68^{KO}$ phenotypes may also arise from putative cytoplasmic functions of SAM68, including the control of mRNA translation (Klein et al., 2015; Klein et al., 2013). We note that with our immunological reagents we could not detect cytoplasmic Sam68 protein in hippocampal neurons. However, considering different reagents or different antigen-accessibility due to experimental protocols, such findings need to be interpreted with caution.

Despite the significant changes in splice isoforms of postsynaptic scaffolding proteins, we did not observe changes in the density or shape of dendritic spines on CA1 pyramidal cells. Thus, the Sam68-dependent alterations in postsynaptic scaffolding proteins may be more important for signalling and plasticity properties of spines rather than their formation. Our observation contrasts a previous report that described a 40% reduction in spine density on primary dendrites with Sam68 loss-of-function (Klein et al., 2013). The reasons for these divergent observations are not clear. However, we note differences in tissue integrity when using different labelling methods (DiOlistic vs. Golgi staining) and differences in the area assessed (primary dendrite vs. higher order branches), mouse strain background, and potentially age of animals used in the two studies.

Another important aspect of our study is the direct comparison of alternative splicing programs regulated by two closely-related paralogues, Sam68 and Slm2. The sequencing and analysis pipeline in this study was exactly the same used previously for exploring Slm2-dependent alternative splicing events in the mouse hippocampus (Traunmüller et al., 2016). Despite the high homology of the RNA-binding domains and identical RNA-binding motifs for Sam68 and Slm2, we did not detect much overlap in the alternative splicing events de-regulated in the respective knock-out mice. Interestingly, we identify several strongly de-regulated splicing events in Sam68 knock-out hippocampus that are essentially unchanged in Slm2 knock-out tissue. On the other hand, several events that are severely de-regulated in Slm2 mutants are only slightly changed in Sam68 mutant mice. Thus, it is unlikely that this apparent target selectivity can be explained by the relative abundance of the RNA binding proteins in the hippocampus. Much rather, it appears that the cellular context and/or signalling state have important impact on the alternative splicing regulation by these STAR

proteins. Notably, previous work highlighted the possibility of differential activities based on heterodimer formation between STAR proteins and additional RNA-binding proteins (RBPs) (Iijima et al., 2014) or the density of binding motifs in target mRNAs (Danilenko et al., 2017). This complexity highlights the challenges of predicting outcomes of alternative splicing regulation based on RBP expression or presence of binding motifs and emphasises the necessity to interrogate alternative splicing programs using cell type-specific methods in the future.

## Supplementary Material

Refer to Web version on PubMed Central for supplementary material.

## Acknowledgements

We are grateful to the Imaging Core Facility and the Proteomic Core Facility of the Biozentrum of the University of Basel for expert assistance, in particular to Erik Ahrné and Alexander Schmidt for help with analysis of mass spectrometry data. We thank Elisabetta Furlanis, Oriane Mauger, Meha Singh, and Thomas Bock for valuable comments on the manuscript. We are indebted to members of the sequencing facility (Philippe Demougin and Christian Beisel), Stephan Peischl from the University of Bern for expert advice on the statistical analysis, Caroline Bornmann and Laetitia Burklé for technical support, the animal care takers and workshops of the Biozentrum of the University of Basel for their dedication and competence, Valerie Besseyrias and Bernhard Bettler for sharing equipment and advice on DiOlistic labeling. D.S. was supported by a FP7 Marie-Curie Mobility Fellowship from the FP7 of the European Union. This work was financially supported by grants to P.S. from the Swiss National Science Foundation, a European Research Council Advanced Grant (SPLICECODE), and the Kanton Basel-Stadt.

## Abbreviations

| | |
|---|---|
| **AS** | Alternative segment |
| **BFDR** | Bayesian False Discovery Rate |
| **CaMKII** | calcium/calmodulin-dependent kinase II |
| **FDR** | false discovery rate |
| **FC** | fold-change |
| **GO** | gene ontology |
| **RBP** | RNA-binding proteins |
| **RT** | room temperature |
| **SAINT analysis** | (significance analysis of interactome analysis) |
| **STAR** | Signal Transduction Associated RNA-binding family of RNA-binding proteins |
| **SI** | splicing index |

## References

Ahrne E, Glatter T, Vigano C, Schubert C, Nigg EA, Schmidt A. Evaluation and Improvement of Quantification Accuracy in Isobaric Mass Tag-Based Protein Quantification Experiments. Journal of proteome research. 2016; 15:2537–2547. [PubMed: 27345528]

Aoto J, Martinelli DC, Malenka RC, Tabuchi K, Südhof TC. Presynaptic neurexin-3 alternative splicing trans-synaptically controls postsynaptic AMPA receptor trafficking. Cell. 2013; 154:75–88. [PubMed: 23827676]

Benjamini Y, Hochberg Y. Controlling the False Discovery Rate: A Practical and Powerful Approach to Multiple Testing. Journal of the Royal Statistical Society. 1995; 57:289–300.

Boucard AA, Chubykin AA, Comoletti D, Taylor P, Sudhof TC. A splice code for trans-synaptic cell adhesion mediated by binding of neuroligin 1 to alpha- and beta-neurexins. Neuron. 2005; 48:229–236. [PubMed: 16242404]

Carlisle HJ, Luong TN, Medina-Marino A, Schenker L, Khorosheva E, Indersmitten T, Gunapala KM, Steele AD, O'Dell TJ, Patterson PH, et al. Deletion of densin-180 results in abnormal behaviors associated with mental illness and reduces mGluR5 and DISC1 in the postsynaptic density fraction. J Neurosci. 2011; 31:16194–16207. [PubMed: 22072671]

Chawla G, Lin CH, Han A, Shiue L, Ares M Jr, Black DL. Sam68 regulates a set of alternatively spliced exons during neurogenesis. Mol Cell Biol. 2009; 29:201–213. [PubMed: 18936165]

Chih B, Gollan L, Scheiffele P. Alternative splicing controls selective trans-synaptic interactions of the neuroligin-neurexin complex. Neuron. 2006; 51:171–178. [PubMed: 16846852]

Choi H, Larsen B, Lin ZY, Breitkreutz A, Mellacheruvu D, Fermin D, Qin ZS, Tyers M, Gingras AC, Nesvizhskii AI. SAINT: probabilistic scoring of affinity purification-mass spectrometry data. Nat Methods. 2011; 8:70–73. [PubMed: 21131968]

Danilenko M, Dalgliesh C, Pagliarini V, Naro C, Ehrmann I, Feracci M, Kheirollahi-Chadegani M, Tyson-Capper A, Clowry GJ, Fort P, et al. Binding site density enables paralog-specific activity of SLM2 and Sam68 proteins in Neurexin2 AS4 splicing control. Nucleic acids research. 2017; 45:4120–4130. [PubMed: 27994030]

de Wit J, Sylwestrak E, O'Sullivan ML, Otto S, Tiglio K, Savas JN, Yates JR 3rd, Comoletti D, Taylor P, Ghosh A. LRRTM2 interacts with Neurexin1 and regulates excitatory synapse formation. Neuron. 2009; 64:799–806. [PubMed: 20064388]

Dobin A, Davis CA, Schlesinger F, Drenkow J, Zaleski C, Jha S, Batut P, Chaisson M, Gingeras TR. STAR: ultrafast universal RNA-seq aligner. Bioinformatics. 2013; 29:15–21. [PubMed: 23104886]

Ehrmann I, Dalgliesh C, Liu Y, Danilenko M, Crosier M, Overman L, Arthur HM, Lindsay S, Clowry GJ, Venables JP, et al. The tissue-specific RNA binding protein T-STAR controls regional splicing patterns of neurexin pre-mRNAs in the brain. PLoS Genet. 2013; 9:e1003474. [PubMed: 23637638]

Eom T, Zhang C, Wang H, Lay K, Fak J, Noebels JL, Darnell RB. NOVA-dependent regulation of cryptic NMD exons controls synaptic protein levels after seizure. eLife. 2013; 2:e00178. [PubMed: 23359859]

Fritschy JM, Harvey RJ, Schwarz G. Gephyrin: where do we stand, where do we go? Trends in neurosciences. 2008; 31:257–264. [PubMed: 18403029]

Furlanis E, Scheiffele P. Regulation of neuronal differentiation, function, and plasticity by alternative splicing. Annual Review of Cell and Developmental Biology. 2018; 34:451–469.

Gan WB, Grutzendler J, Wong WT, Wong RO, Lichtman JW. Multicolor "DiOlistic" labeling of the nervous system using lipophilic dye combinations. Neuron. 2000; 27:219–225. [PubMed: 10985343]

Gandoura S, Weiss E, Rautou PE, Fasseu M, Gustot T, Lemoine F, Hurtado-Nedelec M, Hego C, Vadrot N, Elkrief L, et al. Gene- and exon-expression profiling reveals an extensive LPS-induced response in immune cells in patients with cirrhosis. J Hepatol. 2013; 58:936–948. [PubMed: 23321315]

Glatter T, Ludwig C, Ahrne E, Aebersold R, Heck AJ, Schmidt A. Large-scale quantitative assessment of different in-solution protein digestion protocols reveals superior cleavage efficiency of tandem Lys-C/trypsin proteolysis over trypsin digestion. Journal of proteome research. 2012; 11:5145–5156. [PubMed: 23017020]

Grange J, Boyer V, Fabian-Fine R, Fredj NB, Sadoul R, Goldberg Y. Somatodendritic localization and mRNA association of the splicing regulatory protein Sam68 in the hippocampus and cortex. J Neurosci Res. 2004; 75:654–666. [PubMed: 14991841]

Hansen RT 3rd, Conti M, Zhang HT. Mice deficient in phosphodiesterase-4A display anxiogenic-like behavior. Psychopharmacology (Berl). 2014; 231:2941–2954. [PubMed: 24563185]

Harvey K, Duguid IC, Alldred MJ, Beatty SE, Ward H, Keep NH, Lingenfelter SE, Pearce BR, Lundgren J, Owen MJ, et al. The GDP-GTP exchange factor collybistin: an essential determinant of neuronal gephyrin clustering. J Neurosci. 2004; 24:5816–5826. [PubMed: 15215304]

Hattori D, Demir E, Kim HW, Viragh E, Zipursky SL, Dickson BJ. Dscam diversity is essential for neuronal wiring and self-recognition. Nature. 2007; 449:223–227. [PubMed: 17851526]

Havekes R, Park AJ, Tolentino RE, Bruinenberg VM, Tudor JC, Lee Y, Hansen RT, Guercio LA, Linton E, Neves-Zaph SR, et al. Compartmentalized PDE4A5 Signaling Impairs Hippocampal Synaptic Plasticity and Long-Term Memory. J Neurosci. 2016; 36:8936–8946. [PubMed: 27559174]

Herweg J, Schwarz G. Splice-specific glycine receptor binding, folding, and phosphorylation of the scaffolding protein gephyrin. J Biol Chem. 2012; 287:12645–12656. [PubMed: 22351777]

Ichtchenko K, Hata Y, Nguyen T, Ullrich B, Missler M, Moomaw C, Sudhof TC. Neuroligin 1: a splice site-specific ligand for beta-neurexins. Cell. 1995; 81:435–443. [PubMed: 7736595]

Iijima T, Iijima Y, Witte H, Scheiffele P. Neuronal cell type-specific alternative splicing is regulated by the KH domain protein SLM1. The Journal of cell biology. 2014; 204:331–342. [PubMed: 24469635]

Iijima T, Wu K, Witte H, Hanno-Iijima Y, Glatter T, Richard S, Scheiffele P. SAM68 regulates neuronal activity-dependent alternative splicing of neurexin-1. Cell. 2011; 147:1601–1614. [PubMed: 22196734]

Ince-Dunn G, Okano HJ, Jensen KB, Park WY, Zhong R, Ule J, Mele A, Fak JJ, Yang C, Zhang C, et al. Neuronal Elav-like (Hu) proteins regulate RNA splicing and abundance to control glutamate levels and neuronal excitability. Neuron. 2012; 75:1067–1080. [PubMed: 22998874]

Kins S, Betz H, Kirsch J. Collybistin, a newly identified brain-specific GEF, induces submembrane clustering of gephyrin. Nature neuroscience. 2000; 3:22–29. [PubMed: 10607391]

Klein ME, Castillo PE, Jordan BA. Coordination between Translation and Degradation Regulates Inducibility of mGluR-LTD. Cell reports. 2015

Klein ME, Younts TJ, Castillo PE, Jordan BA. RNA-binding protein Sam68 controls synapse number and local beta-actin mRNA metabolism in dendrites. Proc Natl Acad Sci U S A. 2013; 110:3125–3130. [PubMed: 23382180]

Lee JA, Tang ZZ, Black DL. An inducible change in Fox-1/A2BP1 splicing modulates the alternative splicing of downstream neuronal target exons. Genes Dev. 2009; 23:2284–2293. [PubMed: 19762510]

Li Q, Zheng S, Han A, Lin CH, Stoilov P, Fu XD, Black DL. The splicing regulator PTBP2 controls a program of embryonic splicing required for neuronal maturation. eLife. 2014; 3:e01201. [PubMed: 24448406]

Lin Q, Taylor SJ, Shalloway D. Specificity and determinants of Sam68 RNA binding. Implications for the biological function of K homology domains. J Biol Chem. 1997; 272:27274–27280. [PubMed: 9341174]

Makeyev EV, Zhang J, Carrasco MA, Maniatis T. The MicroRNA miR-124 Promotes Neuronal Differentiation by Triggering Brain-Specific Alternative Pre-mRNA Splicing. Molecular Cell. 2007; 27:435–448. [PubMed: 17679093]

Matsuda K, Budisantoso T, Mitakidis N, Sugaya Y, Miura E, Kakegawa W, Yamasaki M, Konno K, Uchigashima M, Abe M, et al. Transsynaptic Modulation of Kainate Receptor Functions by C1q-like Proteins. Neuron. 2016; 90:752–767. [PubMed: 27133466]

Matter N, Herrlich P, Konig H. Signal-dependent regulation of splicing via phosphorylation of Sam68. Nature. 2002; 420:691–695. [PubMed: 12478298]

Matthews BJ, Kim ME, Flanagan JJ, Hattori D, Clemens JC, Zipursky SL, Grueber WB. Dendrite self-avoidance is controlled by Dscam. Cell. 2007; 129:593–604. [PubMed: 17482551]

Mauger O, Scheiffele P. Beyond proteome diversity: alternative splicing as a regulator of neuronal transcript dynamics. Curr Opin Neurobiol. 2017; 45:162–168. [PubMed: 28609697]

McGlincy NJ, Smith CWJ. Alternative splicing resulting in nonsense-mediated mRNA decay: what is the meaning of nonsense? Trends in biochemical sciences. 2008; 33:385–393. [PubMed: 18621535]

Mi H, Muruganujan A, Casagrande JT, Thomas PD. Large-scale gene function analysis with the PANTHER classification system. Nature protocols. 2013; 8:1551–1566. [PubMed: 23868073]

Nguyen TM, Schreiner D, Xiao L, Traunmuller L, Bornmann C, Scheiffele P. An alternative splicing switch shapes neurexin repertoires in principal neurons versus interneurons in the mouse hippocampus. eLife. 2016; 5

Nilsen TW, Graveley BR. Expansion of the eukaryotic proteome by alternative splicing. Nature. 2010; 463:457–463. [PubMed: 20110989]

Noli L, Capalbo A, Ogilvie C, Khalaf Y, Ilic D. Discordant Growth of Monozygotic Twins Starts at the Blastocyst Stage: A Case Study. Stem Cell Reports. 2015; 5:946–953. [PubMed: 26584541]

Parikshak NN, Swarup V, Belgard TG, Irimia M, Ramaswami G, Gandal MJ, Hartl C, Leppa V, Ubieta LT, Huang J, et al. Genome-wide changes in lncRNA, splicing, and regional gene expression patterns in autism. Nature. 2016; 540:423–427. [PubMed: 27919067]

Paronetto MP, Achsel T, Massiello A, Chalfant CE, Sette C. The RNA-binding protein Sam68 modulates the alternative splicing of Bcl-x. The Journal of cell biology. 2007; 176:929–939. [PubMed: 17371836]

Paz I, Kosti I, Ares M Jr, Cline M, Mandel-Gutfreund Y. RBPmap: a web server for mapping binding sites of RNA-binding proteins. Nucleic acids research. 2014; 42:W361–367. [PubMed: 24829458]

Quesnel-Vallieres M, Dargaei Z, Irimia M, Gonatopoulos-Pournatzis T, Ip JY, Wu M, Sterne-Weiler T, Nakagawa S, Woodin MA, Blencowe BJ, et al. Misregulation of an Activity-Dependent Splicing Network as a Common Mechanism Underlying Autism Spectrum Disorders. Mol Cell. 2016; 64:1023–1034. [PubMed: 27984743]

Quesnel-Vallieres M, Irimia M, Cordes SP, Blencowe BJ. Essential roles for the splicing regulator nSR100/SRRM4 during nervous system development. Genes Dev. 2015; 29:746–759. [PubMed: 25838543]

Raj B, Blencowe BJ. Alternative Splicing in the Mammalian Nervous System: Recent Insights into Mechanisms and Functional Roles. Neuron. 2015; 87:14–27. [PubMed: 26139367]

Ray D, Kazan H, Cook KB, Weirauch MT, Najafabadi HS, Li X, Gueroussov S, Albu M, Zheng H, Yang A, et al. A compendium of RNA-binding motifs for decoding gene regulation. Nature. 2013; 499:172–177. [PubMed: 23846655]

Richard S, Torabi N, Franco GV, Tremblay GA, Chen T, Vogel G, Morel M, Cleroux P, Forget-Richard A, Komarova S, et al. Ablation of the Sam68 RNA binding protein protects mice from age-related bone loss. PLoS Genet. 2005; 1:e74. [PubMed: 16362077]

Saito Y, Miranda-Rottmann S, Ruggiu M, Park CY, Fak JJ, Zhong R, Duncan JS, Fabella BA, Junge HJ, Chen Z, et al. NOVA2-mediated RNA regulation is required for axonal pathfinding during development. eLife. 2016; 5

Sanchez-Jimenez F, Sanchez-Margalet V. Role of Sam68 in post-transcriptional gene regulation. Int J Mol Sci. 2013; 14:23402–23419. [PubMed: 24287914]

Sando R, Bushong E, Zhu Y, Huang M, Considine C, Phan S, Ju S, Uytiepo M, Ellisman M, Maximov A. Assembly of Excitatory Synapses in the Absence of Glutamatergic Neurotransmission. Neuron. 2017; 94:312–321 e313. [PubMed: 28426966]

Schmucker D, Clemens JC, Shu H, Worby CA, Xiao J, Muda M, Dixon JE, Zipursky SL. Drosophila Dscam is an axon guidance receptor exhibiting extraordinary molecular diversity. Cell. 2000; 101:671–684. [PubMed: 10892653]

Schreiner D, Nguyen T-M, Russo G, Hebr S, Patrignani A, Ahrné E, Scheiffele P. Targeted Combinatorial Alternative Splicing Generates Brain Region-Specific Repertoires of Neurexins. Neuron. 2014

Schreiner D, Simicevic J, Ahrné E, Schmidt A, Scheiffele P. Quantitative isoform-profiling of highly diversified recognition molecules. eLife. 2015; 4:1–17.

Sigler A, Oh WC, Imig C, Altas B, Kawabe H, Cooper BH, Kwon HB, Rhee JS, Brose N. Formation and Maintenance of Functional Spines in the Absence of Presynaptic Glutamate Release. Neuron. 2017; 94:304–311 e304. [PubMed: 28426965]

Staffend NA, Meisel RL. DiOlistic labeling in fixed brain slices: phenotype, morphology, and dendritic spines. Current protocols in neuroscience / editorial board, Jacqueline N Crawley [et al]. 2011; Chapter 2:Unit 2 13.

Stoss O, Novoyatleva T, Gencheva M, Olbrich M, Benderska N, Stamm S. p59 (fyn)-mediated phosphorylation regulates the activity of the tissue-specific splicing factor rSLM-1. Mol Cell Neurosci. 2004; 27:8–21. [PubMed: 15345239]

Strack S, Robison AJ, Bass MA, Colbran RJ. Association of calcium/calmodulin-dependent kinase II with developmentally regulated splice variants of the postsynaptic density protein densin-180. J Biol Chem. 2000; 275:25061–25064. [PubMed: 10827168]

Sun W, You X, Gogol-Doring A, He H, Kise Y, Sohn M, Chen T, Klebes A, Schmucker D, Chen W. Ultra-deep profiling of alternatively spliced Drosophila Dscam isoforms by circularization-assisted multi-segment sequencing. EMBO J. 2013; 32:2029–2038. [PubMed: 23792425]

Taniguchi H, Gollan L, Scholl FG, Mahadomrongkul V, Dobler E, Limthong N, Peck M, Aoki C, Scheiffele P. Silencing of neuroligin function by postsynaptic neurexins. J Neurosci. 2007; 27:2815–2824. [PubMed: 17360903]

Traunmüller L, Bornmann C, Scheiffele P. Alternative splicing coupled nonsense-mediated decay generates neuronal cell type-specific expression of SLM proteins. J Neurosci. 2014; 34:16755–16761. [PubMed: 25505328]

Traunmüller L, Gomez AM, Nguyen T-M, Scheiffele P. Control of neuronal synapse specification by highly dedicated alternative splicing program. Science. 2016; 352:982–986. [PubMed: 27174676]

Uemura T, Lee SJ, Yasumura M, Takeuchi T, Yoshida T, Ra M, Taguchi R, Sakimura K, Mishina M. Trans-synaptic interaction of GluRdelta2 and Neurexin through Cbln1 mediates synapse formation in the cerebellum. Cell. 2010; 141:1068–1079. [PubMed: 20537373]

Ule J, Jensen KB, Ruggiu M, Mele A, Ule A, Darnell RB. CLIP identifies Nova-regulated RNA networks in the brain. Science. 2003; 302:1212–1215. [PubMed: 14615540]

Ule J, Ule A, Spencer J, Williams A, Hu JS, Cline M, Wang H, Clark T, Fraser C, Ruggiu M, et al. Nova regulates brain-specific splicing to shape the synapse. Nat Genet. 2005; 37:844–852. [PubMed: 16041372]

Vogel G, Richard S. Emerging roles for Sam68 in adipogenesis and neuronal development. RNA Biol. 2012; 9:1129–1133. [PubMed: 23018781]

Vuong CK, Black DL, Zheng S. The neurogenetics of alternative splicing. Nature reviews Neuroscience. 2016; 17:265–281. [PubMed: 27094079]

Wang ET, Cody NA, Jog S, Biancolella M, Wang TT, Treacy DJ, Luo S, Schroth GP, Housman DE, Reddy S, et al. Transcriptome-wide regulation of pre-mRNA splicing and mRNA localization by muscleblind proteins. Cell. 2012; 150:710–724. [PubMed: 22901804]

Wang ET, Sandberg R, Luo S, Khrebtukova I, Zhang L, Mayr C, Kingsmore SF, Schroth GP, Burge CB. Alternative isoform regulation in human tissue transcriptomes. Nature. 2008; 456:470–476. [PubMed: 18978772]

Wang S, Stanika RI, Wang X, Hagen J, Kennedy MB, Obermair GJ, Colbran RJ, Lee A. Densin-180 Controls the Trafficking and Signaling of L-Type Voltage-Gated Cav1.2 Ca(2+) Channels at Excitatory Synapses. J Neurosci. 2017; 37:4679–4691. [PubMed: 28363979]

Yap K, Lim ZQ, Khandelia P, Friedman B, Makeyev EV. Coordinated regulation of neuronal mRNA steady-state levels through developmentally controlled intron retention. Genes & development. 2012; 26:1209–1223. [PubMed: 22661231]

Yoon KJ, Lee HR, Jo YS, An K, Jung SY, Jeong MW, Kwon SK, Kim NS, Jeong HW, Ahn SH, et al. Mind bomb-1 is an essential modulator of long-term memory and synaptic plasticity via the Notch signaling pathway. Mol Brain. 2012; 5:40. [PubMed: 23111145]

Zhang Y, Chen K, Sloan SA, Bennett ML, Scholze AR, O'Keeffe S, Phatnani HP, Guarnieri P, Caneda C, Ruderisch N, et al. An RNA-sequencing transcriptome and splicing database of glia, neurons, and vascular cells of the cerebral cortex. J Neurosci. 2014; 34:11929–11947. [PubMed: 25186741]

Zheng S, Black DL. Alternative pre-mRNA splicing in neurons: growing up and extending its reach. Trends Genet. 2013; 29:442–448. [PubMed: 23648015]

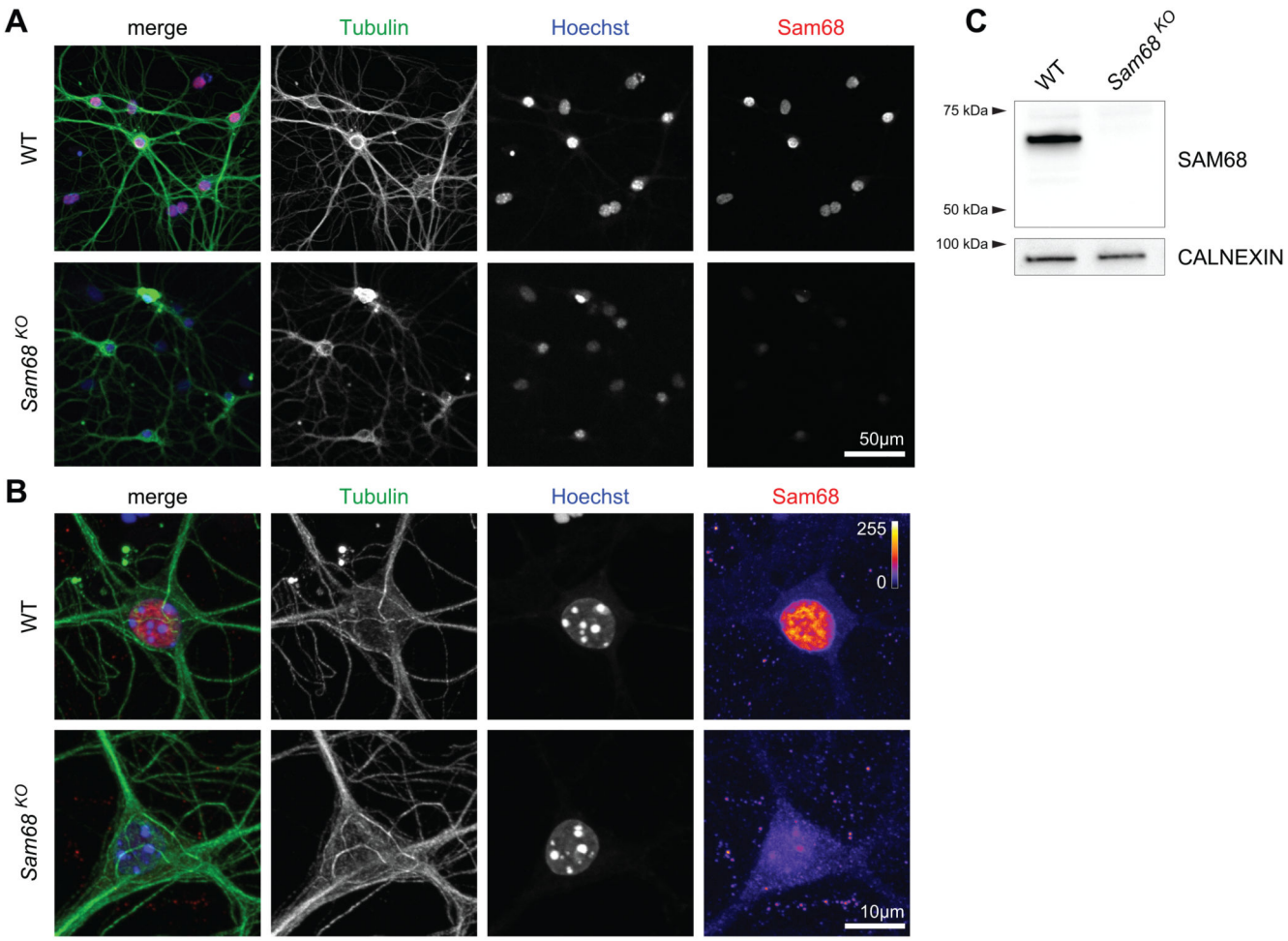


**Figure 1. Subcellular localization of Sam68**

A, B) Cultured dissociated hippocampal neurons (12 days *in vitro* (DIV 12) from WT and Sam68 knock-out (KO) P0 animals. Distribution of Sam68 was assessed by co-immunostaining for neuron-specific tubulin and Sam68, nuclei were visualized by Hoechst staining. In the high-magnification image in (B) Sam68 is shown using a false color lookup tabe (LUT) for better visualization. Notably, a vast majority of Sam68 shows nuclear localization.

Scale bars 50µm (A), 10µm (B).

C) Confirmation of anti-Sam68 antibody specificity (mouse whole brain lysates, adult WT and *Sam68*$^{KO}$). Calnexin is used as loading control. Representative Western Blot of n>3 experiments is shown.




Europe PMC Funders Author Manuscripts

Europe PMC Funders Author Manuscripts

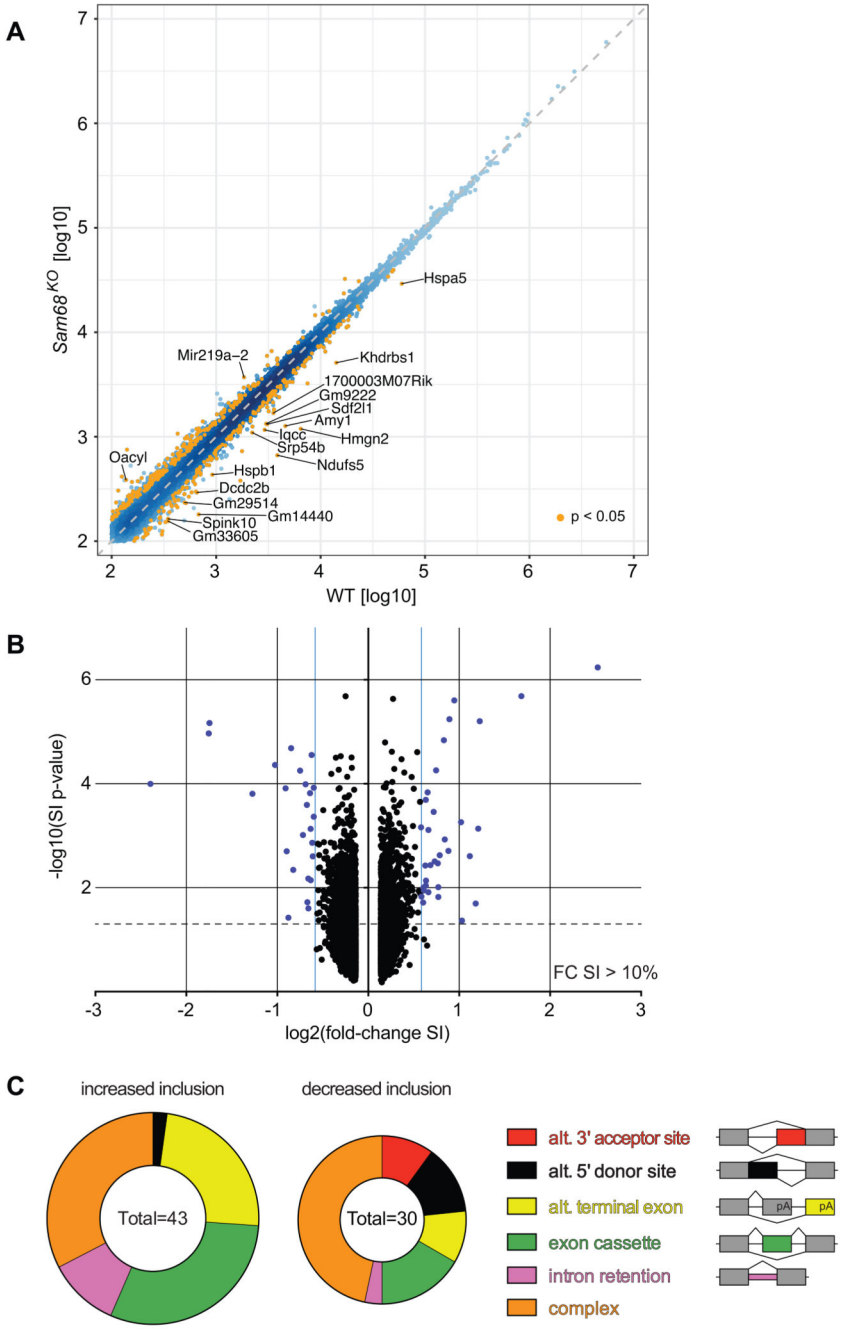


**Figure 2. RNA deep sequencing assessment of *Sam68*$^{KO}$**

A) Scatter plot of normalized gene expression (Log10-scale) for WT and *Sam68*$^{KO}$ (n = 4 hippocampal samples, age P30; cut-off DESeq normalized expression > 100). ($R^2$ = 0.9924, Pearson correlation coefficient). Genes highlighted in orange show adjusted p-values of <0.05. Selected genes with p<0.05 and fold-change (FC) > 2 are annotated.

B) Volcano plot of fold change (FC) of splicing index (SI) and p-values for all exons with an FC SI > 10% (total of 9110 exons).

Vertical blue lines indicate a FC of ±1.50, dashed horizontal line indicates p=0.05. Values highlighted in dark blue show a significant ($p<0.05$) fold-change of ≥ 1.50

C) Pie chart of alternative splicing events with significantly ($p<0.05$; FC SI ≥ 1.50) increased (left) or decreased (right) inclusion in Sam68-deficient animals, plotted by event class. Schematic representations of splicing events are shown on the right. pA indicates poly-adenylation sites.



Europe PMC Funders Author Manuscripts

Europe PMC Funders Author Manuscripts

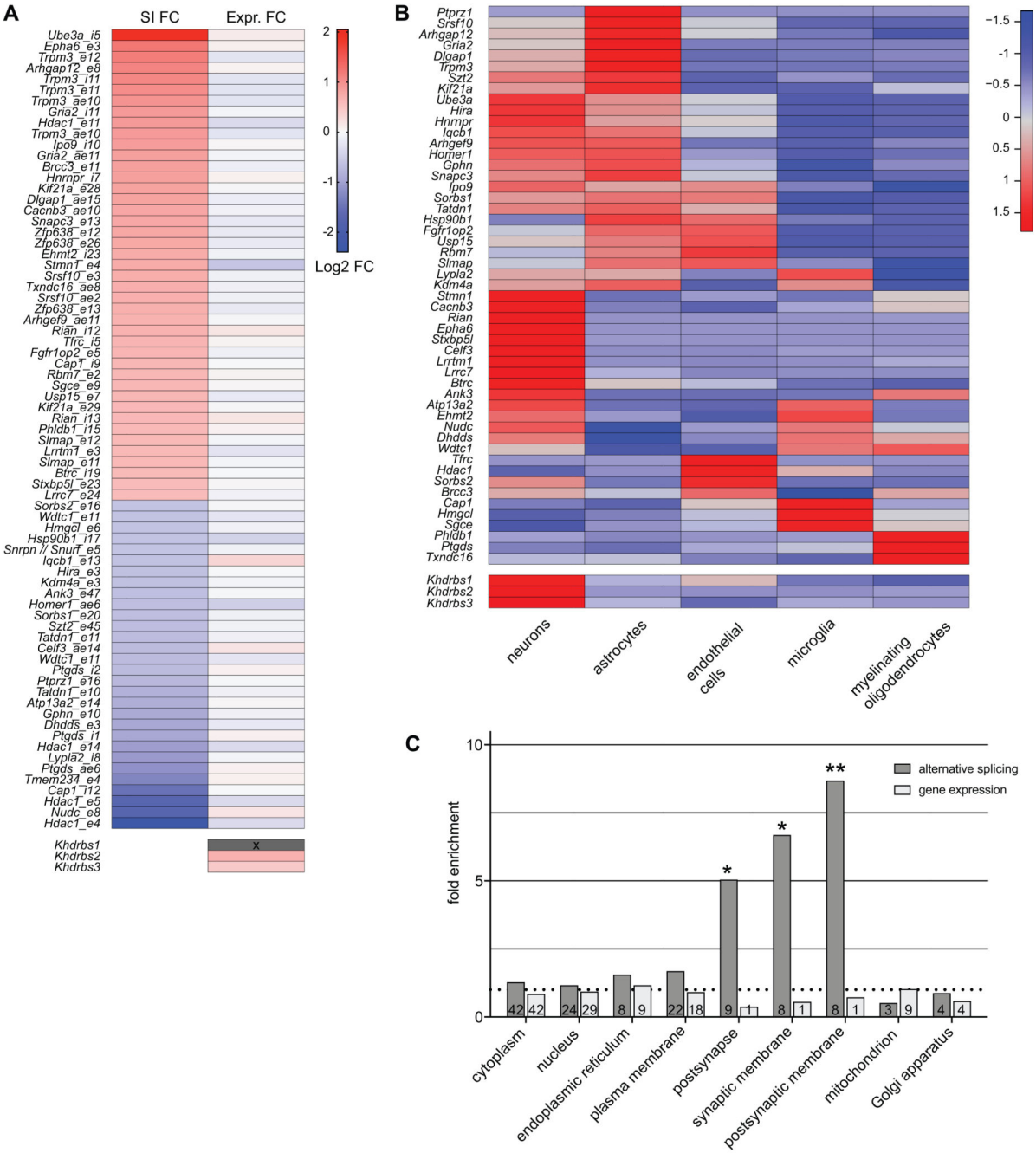


**Figure 3. Classification of *Sam68*$^{KO}$ target genes**

A) Heat map of significant (FC SI ≥ 1.50, p<0.05) alternative splicing events vs. corresponding changes in expression level (log2-scale) in hippocampal samples of *Sam68*$^{KO}$ compared to WT. Changes in overall expression level of Sam68 target genes are small.

B) Heat map of cell type-specificity of expression of genes showing Sam68-dependent alternative splicing. Expression levels were assessed using expression data from cortical neurons (Zhang et al., 2014). Expression is displayed mean-centered per row.

C) Analysis of the GO cellular component-association of Sam68 alternative splicing targets using the PANTHER classification system (Overrepresentation Test). Numbers of genes in the lists of Sam68 alternative splicing targets and gene expression changes, respectively, are displayed. Adjusted p-values (Fisher's Exact test with FDR multiple test correction) are 0.0326, 0.0249, and 0.0078 for GO terms postsynapse (GO:0098794), synaptic membrane (GO:0097060), and postsynaptic membrane (GO:0045211), respectively.



Europe PMC Funders Author Manuscripts

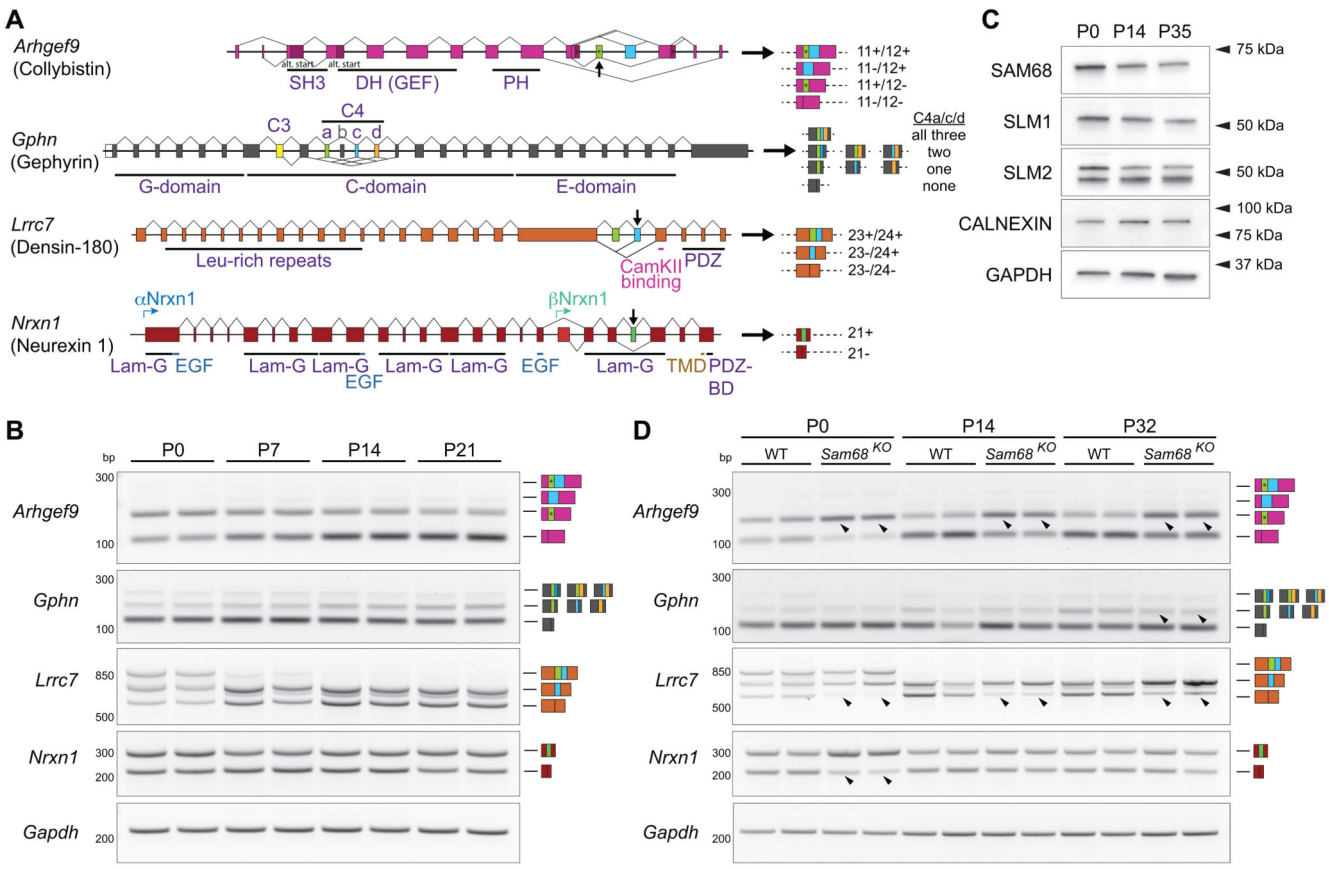


**Figure 4. Sam68-dependent alternative splicing of synaptic components**

A) Schematic gene structure representation of four Sam68 alternative splicing targets: *Arhgef9* (Collybistin), *Gphn* (gephyrin), *Lrrc7* (Densin-180), and *Nrxn1* (Neurexin 1) Sam68-dependent alternative segments are highlighted in colours different from constitutive exons. Stop codons are indicated by asterisks for Arhgef9. Stable exon IDs or genomic positions (GRCm38/mm10) are: *Arhgef9* exon 11: ENSMUSE00000817669, *Arhgef9* exon 12 ENSMUSE00000697324; *Gphn* exon 10 (splice cassette C4a; Fritschy *et al.*, 2008, PMID 18403029): ENSMUSE00000418916, *Gphn* exon 11 (C4c): ENSMUSE00000418905, *Gphn* exon 12 (C4d): chr12:78560360-78560422; *Lrrc7* exon 23: ENSMUSE00000668385, *Lrrc7* exon 24: ENSMUSE00000440890; *Nrxn1* exon 21 (AS4): ENSMUSE00001309616.

The *Gphn* C4 cluster (Fritschy et al., 2008) is particularly complex with multiple alternative exon cassettes C4a-d. In our validation experiments, C4b isoforms were not significantly detected.

Exons and introns are not depicted to scale.

B) Developmental time course of *Arhgef9*, *Gphn*, *Lrrc7*, and *Nrxn1* at P0, P7, P14 and P21 in WT animals (mouse hippocampus). Representative RT-PCR of n=3 independent experiments is shown. Identity of PCR products was confirmed by TOPO-cloning and DNA sequencing. Individual bands for gephyrin single and double C4 insertions were mixed products of C4a,c,d exons that could not be electrophoretically resolved.




Europe PMC Funders Author Manuscripts

C) Expression of STAR-proteins in hippocampus during the first five weeks of postnatal development (P0, P14, and P35). Calnexin and Gapdh are used as loading controls. Western blot representative of n=3 independent experiments is shown.
D) Comparison of alternative splicing patterns in hippocampus during the first four to five weeks of postnatal development (P0, P14, and P32) for WT and *Sam68*$^{KO}$. Marked changes are highlighted by arrow heads for selected time points. Representative RT-PCR of n>4 independent experiments is shown.


Europe PMC Funders Author Manuscripts

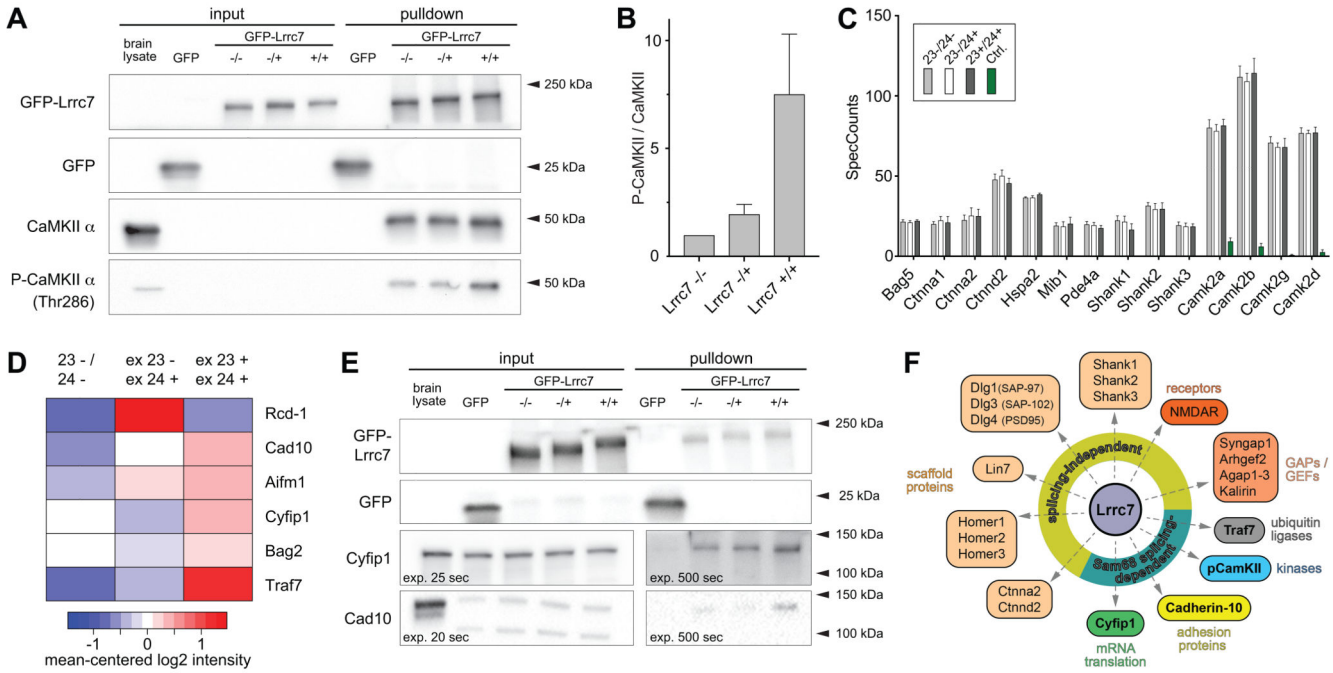


**Figure 5. Functional relevance of Lrrc7 protein isoforms**

A) Affinity isolation of Lrrc7 interaction partners. GFP-tagged full length Lrrc7 isoforms lacking (-) or containing (+) domains encoded by exon 23 and 24 were expressed in HEK293T cells, affinity purified and used to isolate Lrrc7 binding partners from whole brain lysate of adult mice (C57BL/6JRj male mice, 12-16 weeks old). [For example, -/+ represents the Lrrc7 protein isoform lacking the domain encoded by exon 23 and containing the domain encoded by exon 24.] CaMKII, a well-characterized interactor of Lrrc7 is robustly recovered. Western blot representative of n=3 independent experiments is shown.

B) Lrrc7 isoform-specific recovery of active CaMKII (phosphorylated on Thr286). Mean intensity values plus standard error are shown. p-values are 0.089 and 0.078 for Lrrc7 -/+ and Lrrc7 +/+, respectively (two-tailed t-test).

C) Mass spectrometry-based analysis of affinity-isolated Lrrc7 interaction partners. Proteins binding to GFP-tagged Lrrc7 were affinity-isolated from adult whole brain lysates (C57BL/6JRj male mice, 12-16 weeks old) on GFP-Lrrc7 isoform matrices and quantified by shotgun mass spectrometry (MS). The ten most significant isoform-independent Lrrc-interaction partners (in alphabetical order), as ranked by SAINT protein-protein interaction confidence score (Choi et al., 2011), are shown, in addition known interaction partners (CaMKII). The number of spectral counts per interaction partner, i.e. the number of confidently identified peptide spectrum matches (PSMs) per protein interactor is displayed. The isoform-specific quantitative read-out is presented per protein; (from left to right); GFP-tagged bait protein Lrrc7 23-/24-, Lrrc7 23-/24+, Lrrc7 23+/24+, and GFP (control). Error bars show the standard deviation of biological replicates (n=4). Technical mass spectrometry replicates were acquired for each biological replicate and the average spectral count per protein was retained.

D) Lrrc7 isoform-specific interaction partners. Heat-map of summed ms1-intensities (log2 scale) per bait and interaction partner. The data is mean-centred per protein interactor, and




Europe PMC Funders Author Manuscripts

biological replicates (n=4) of each bait experiment are represented by the average intensity. The displayed interaction partners are those that were found to be isoform-specific i.e, significantly differentially abundant (Benjamini-Hochberg adjusted moderated t-test p-value < 0.05) in at least one bait-bait condition comparison (SafeQuant).
E) Validation of isoform-specific Lrrc7 interactions by Western Blot. Recovery of Cyfip1 and Cadherin 10 by pulldown was moderate, thus extended exposures of the pulldown fractions are shown. Western blot representative of n=3 independent experiments is shown.
F) Selected interactors of Lrrc7 / Densin-180. Densin-180 engages in interactions with multiple binding partners including scaffold proteins, receptors, GTPase-activating proteins and guanine nucleotide exchange factors (GAPs / GEFs), ubiquitin ligases, kinases, adhesion proteins, and regulators of mRNA translation. A majority of these interactions are splicing-independent, i.e. independent of the splice variant of Densin-180 involved. Sam68 regulates the alternative splicing of Lrrc7/Densin-180 at the alternatively spliced segment exon 23 / 24. The Densin-180 domains encoded by these domains modulate the interaction with an important subset of binding partners.


Europe PMC Funders Author Manuscripts

Europe PMC Funders Author Manuscripts

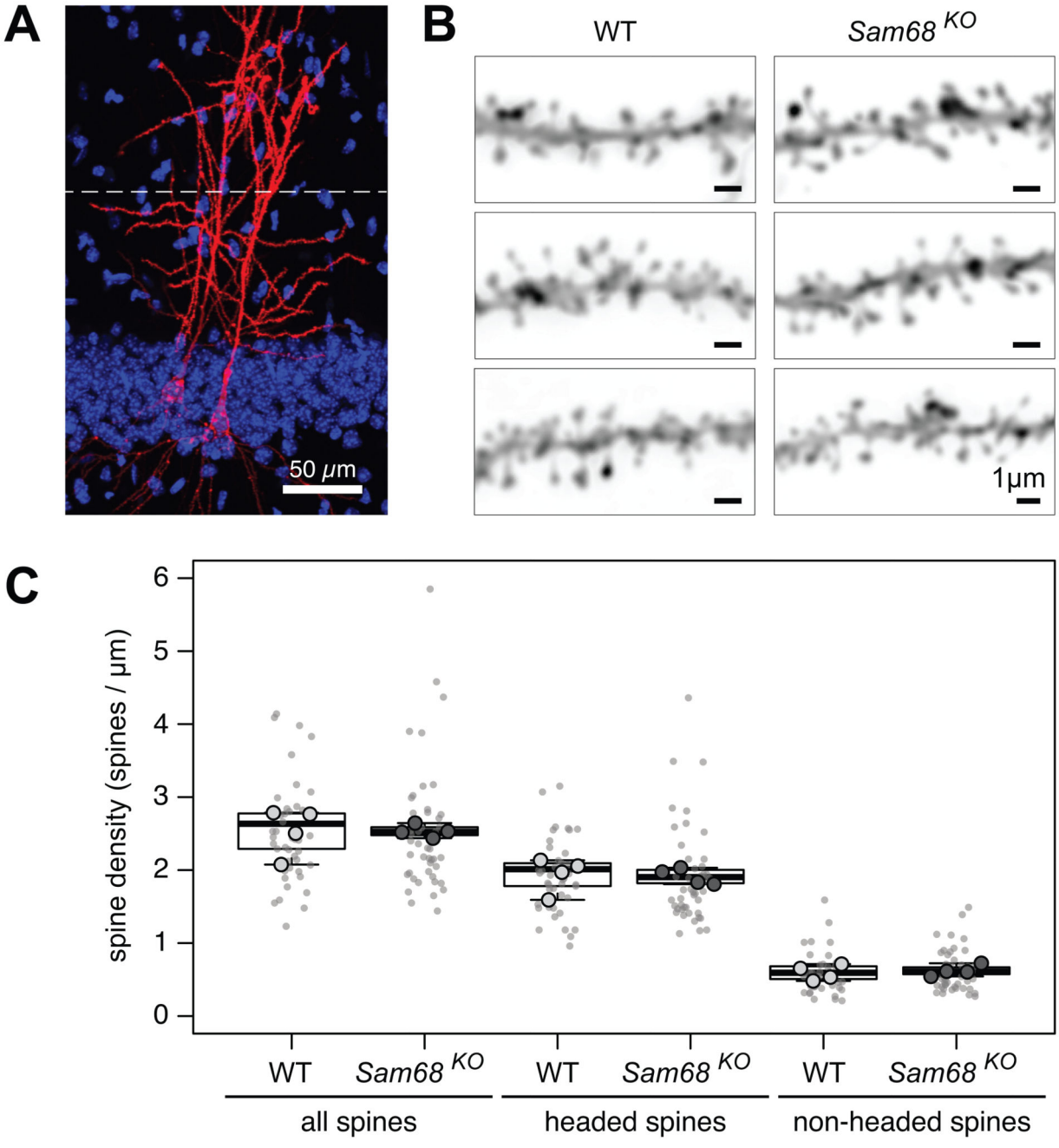


**Figure 6. Assessment of spine density in *Sam68*$^{KO}$ hippocampus**

A) DiOlistic labelling of CA1 hippocampal neurons. Individual neurons were labelled using DiI dye, nuclei were visualized using Hoechst dye to ensure assessment of pyramidal neurons. Spine density on higher order branches of dendrites of CA1 neurons in the stratum radiatum was evaluated on 150μm sagittal sections. Dashed line indicates 100μm distance from stratum pyramidale. Scale bar represents 50μm.

B) High magnification images of representative examples of DiOlistic labelling of pyramidal neuron spines. Examples shown are from three independent littermate pairs (WT and *Sam68*$^{KO}$). Scale bars represent 1μm.

C) Spine density of headed and non-headed spines as assessed by confocal microscopy. Light points indicate individual counts, circles indicate animal means. n = 4 littermates (WT/*Sam68*$^{KO}$) per genotype, animal age P32.



Europe PMC Funders Author Manuscripts

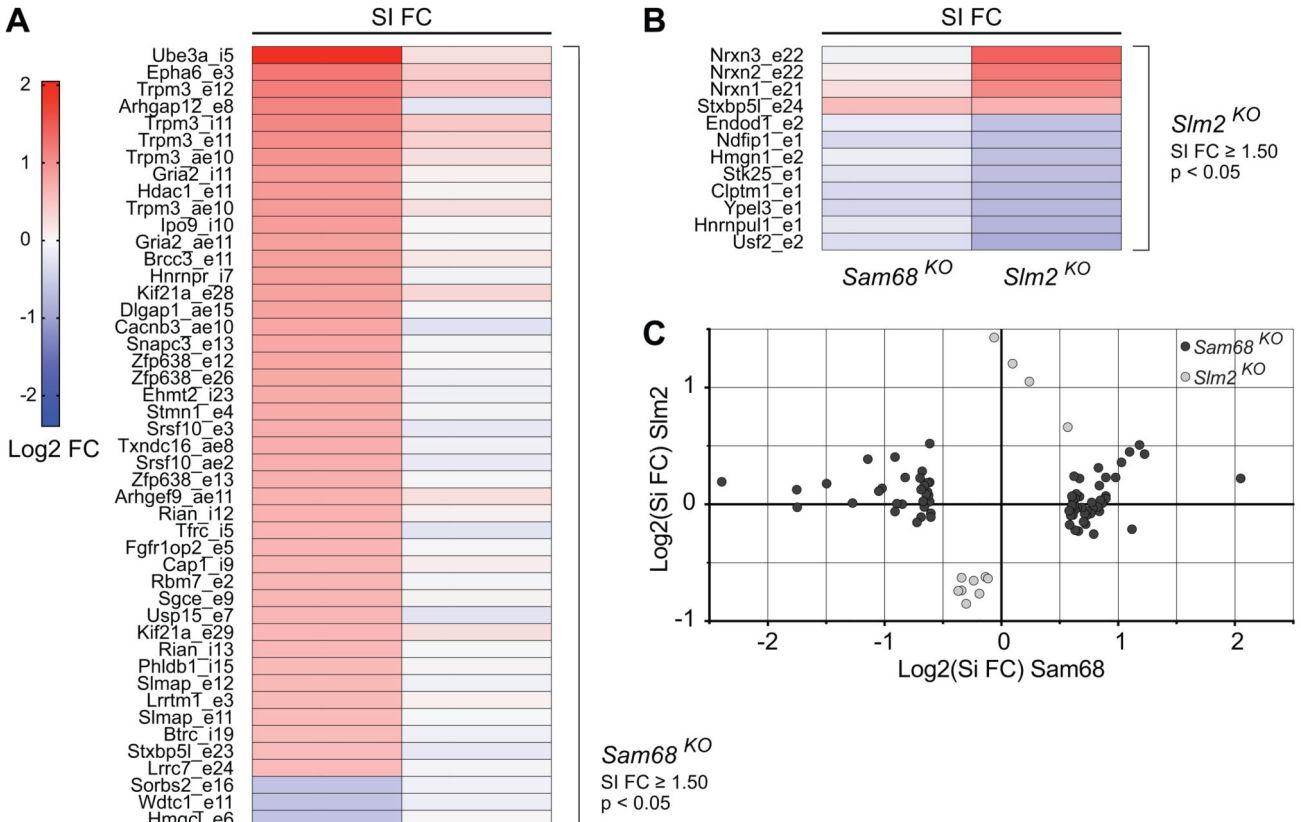


**Figure 7. Target specificity of STAR proteins**

A, B) Heat maps of fold changes (FC) in splicing index (SI) of Sam68 targets (this study) compared to targets of Slm2 (Traunmüller et al., 2016). Targets of Sam68 were only slightly changed in *Slm2*$^{KO}$ animals (A). Likewise, alternative splicing of targets of Slm2 was hardly changed in *Sam68*$^{KO}$ animals (B).

C) Scatter plot of direct comparison of SI FC of Sam68 (black) and Slm2 (grey) targets. Log2 values of SI FC is shown.




Europe PMC Funders Author Manuscripts